Secondary instabilities of convection in a shallow cavity

By TZYY-MING WANG and SEPPO A. KORPELA

Department of Mechanical Engineering, The Ohio State University, 206 West 18th Avenue,
Columbus, OH 43210, USA

Analysis of secondary instabilities of natural convection in a shallow cavity heated from a side has been carried out. For mercury with Prandtl number equal to 0.027 analysis of the primary instabilities by linear theory shows that an instability sets in as transverse cells at Grashof number equal to 9157.6. Instability resulting in oscillatory longitudinal rolls is also possible, their critical Grashof number being equal to 10608.4. The secondary instabilities of the equilibrium states of transverse cells for mercury have been determined. The results show roughly that stable transverse cells with wavelength shorter than the critical become unstable by subharmonic resonance, but the instability for longer cells sets in by a combination resonance. The instability as longitudinal oscillatory rolls reappears at larger values of Grashof number, although slightly delayed by the presence of the transverse cells.

1. Introduction

The characteristics of natural convection in a shallow cavity heated from a side have been under study during the past twenty years owing to the connection of this kind of flow to those in atmospheres, estuaries, ventilation of buildings, and growing of crystals. Here we consider its *secondary instabilities*. The work on the primary instabilities of this convective flow was begun by Hart (1972), who discovered a parallel flow solution for it in the limiting case of an infinitely shallow cavity and drew attention to its relationship to Hadley circulation in the atmosphere. He found, using linear theory, that the instability sets in, either as stationary transverse cells, or as oscillatory longitudinal rolls, depending on the value of the Prandtl number. In a later study Hart (1983) reconsidered the stability of Hadley circulations, now with a free surface or with insulated thermal conditions for the top and bottom plates. The stability analysis of the longitudinal rolls was taken up also by Gill (1974), who related his findings to the observations by Hurle (1966) and Hurle, Jakeman & Johnson (1974) that oscillatory flows exist in melts in the containers used to grow semiconductor crystals, and that oscillations in concentration are responsible for striations in the crystals grown in this way.

The stability calculations were repeated by Roux, Bontoux & Henry (1984) and by Kuo *et al.* (1986). They corrected some inaccuracies in the earlier results and in subsequent studies the structure of both the transverse cells (Laure 1987; Kuo & Korpela 1988) and longitudinal rolls (Laure 1987; Wang & Korpela 1989) were investigated. Actually, the primary stability had already been completely analysed by Gershuni, Zhukhovitskii & Myznikov (1974), but their paper had been overlooked by the later workers.

An important secondary instability analysis that bears on our study was carried

out by Nagata & Busse (1983) for a flow of a fluid with a vanishing Prandtl number *Pr* in an inclined cavity. Despite the flow being heated in a different way, the instability of this flow takes place identically to that discussed here, if the Prandtl number is set to zero. The effects on secondary instability of having the Prandtl number equal to that of air ($Pr = 0.71$) were considered by Chait & Korpela (1989) for natural convection in a vertical cavity.

Related flows in free shear layers, that also have inflexional velocity profiles, have been studied by Kelly (1967) in a seminal paper that stresses the importance of parametric resonance as a mechanism for secondary instability. Later studies by Pierrehumbert & Widnall (1982) and Klaassen & Peltier (1989), based on Floquet theory, further elucidate the pairing of Kelvin–Helmholtz billows and the latter also takes into account the density stratification.

Experimental studies of the flow in a shallow cavity include those of Hart (1983) and Hung & Andereck (1988). Both used mercury as a working fluid and found oscillations similar to those identified by Hurle (1966). In order to relate the theory and the experiments to each other, the results given here are for flow of mercury in a cavity with insulated top and bottom boundaries. It has turned out that low-Prandtl-number flows have the richest structure and are from the point of view of crystal growth the most important technologically. For them the primary stability analysis predicts a transition to transverse cells whenever the Prandtl number is less than 0.033. For larger values of *Pr* the secondary flow consists of oscillatory longitudinal rolls. For mercury, with $Pr = 0.027$, the transverse cells appear at Grashof number equal to 9157.6 and the onset of oscillatory longitudinal rolls at the slightly larger value $Gr = 10608.4$. In the studies of a flow in a vertical cavity Nagata & Busse (1983) and Chait & Korpela (1989) found that the transverse cells in that case soon become unstable by the mechanism of subharmonic resonance. We expected the same to be true here and thus undertook the determination of the stability of the transverse cells for mercury in the range of Grashof numbers between the onset of transverse cells and longitudinal rolls.

2. Formulation

Natural convection in a shallow cavity as shown in figure 1, with top and bottom boundaries made of insulating material, is considered. A Newtonian fluid is assumed to occupy the cavity which is heated from its right side. A right-handed coordinate system is fixed to the cavity in such a way that the *x*-axis points in the direction of the background temperature gradient and *y*-direction is perpendicular to the two horizontal solid boundaries and opposite to gravity. The *z*-coordinate is in the direction of the span, which is taken, as *x*, to be of infinite extent.

The flow is assumed to be governed by the continuity, the Boussinesq form of the Navier–Stokes equations, and the thermal energy balance. These are

$$\nabla \cdot V = 0, \tag{2.1}$$

$$\partial V/\partial t + Gr(V \cdot \nabla) V = -Gr\nabla P + T\hat{j} + \nabla^2 V, \tag{2.2}$$

$$\partial T/\partial t + Gr(V \cdot \nabla) T = 1/Pr \, \nabla^2 T. \tag{2.3}$$

In these equations *V*, *T*, and *P* are the non-dimensional velocity vector, temperature and pressure. These variables have been put into a non-dimensional form by dividing lengths, velocities, time, and pressure by *H*, $U_c = g\gamma s H^3/\nu$, H^2/ν and ρU_c^2,
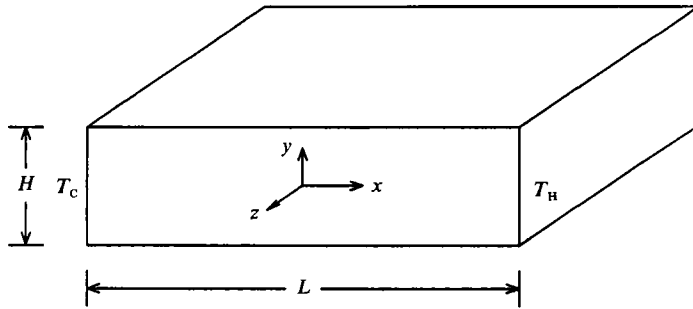
FIGURE 1. A sketch of a shallow cavity.

respectively, where H is the cavity height, g is the gravitational acceleration, s is the background temperature gradient, γ is the coefficient of volumetric expansion and, ν is the kinematic viscosity. The temperature is measured above the mean temperature of the two endwalls and is scaled by the factor sH. The parameters $Gr = U_c H/\nu$ and $Pr = \nu/\kappa$ are the Grashof and Prandtl numbers, respectively. In the definition of Prandtl number κ is the thermal diffusivity.

2.1. *Base flow*

Since both x- and z-directions are taken to be infinitely long, the ends do not influence the flow. That is, we are only concerned with the central region of this cavity. With this idealization, the flow in the central part of the cavity is strictly parallel and Hart (1972) has shown that for insulated top and bottom boundaries the solution is given by

$$u_{\mathrm{b}} = \tfrac{1}{6} y(y^2 - \tfrac{1}{4}), \tag{2.4}$$

$$T_{\mathrm{b}} = x + \tfrac{1}{120} Pr \, Gr \, y(y^4 - \tfrac{5}{6}y^2 + \tfrac{5}{16}). \tag{2.5}$$

The subscript b is appended to the x-component of the velocity and the temperature to signify that these variables represent the base flow.

2.2. *Primary flow stability and the secondary flow*

The shear flow described by (2.4) and (2.5) is known to go unstable at sufficiently large values of the Grashof number. We have calculated the neutral states for mercury with $Pr = 0.027$ and show them in figure 2. At the onset of instability steady transverse cells set in at $Gr = 9157.6$. The periodicity in the x-direction is given at the critical state by the wavenumber $\alpha = 2.7$. The maximum amplification rates at supercritical states occur at a slightly lower value of wavenumber, but the deviation is so slight that one cannot use it with any confidence as a guide to determine whether the wavelength increases or decreases as the amplitude of convection becomes larger. Direct numerical calculations by Drummond & Korpela (1987) for a flow in a finite cavity show, however, that the wavelength increases slightly.

On the left side of figure 2 the contour lines show that longitudinal modes could set in at $Gr = 10\,608.4$ with $\beta = 0.7$. No contour lines were drawn beyond $Gr = 18\,000$, which is the reason why white areas appear in the plot. The bi-modality of the instability is very clear, for the valleys and peaks in the plot are distinct.

In order to carry out the secondary instability analysis of the transverse cells, the secondary flow was first calculated numerically. To this end each of the variables in the governing equations (2.1)–(2.3) were split into a part representing the base flow
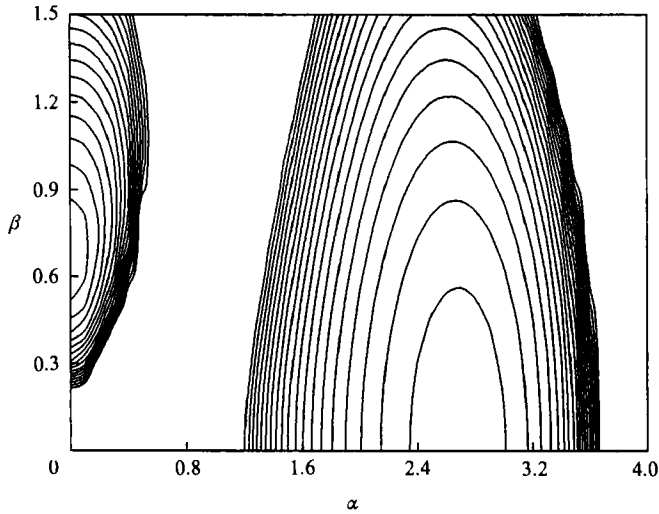
FIGURE 2. The contour lines of Grashof number at neutral states of mercury with $Pr = 0.027$. The contour lines, beginning from $Gr = 9500$, are in increments of 500, with the last for $Gr = 18\,000$.
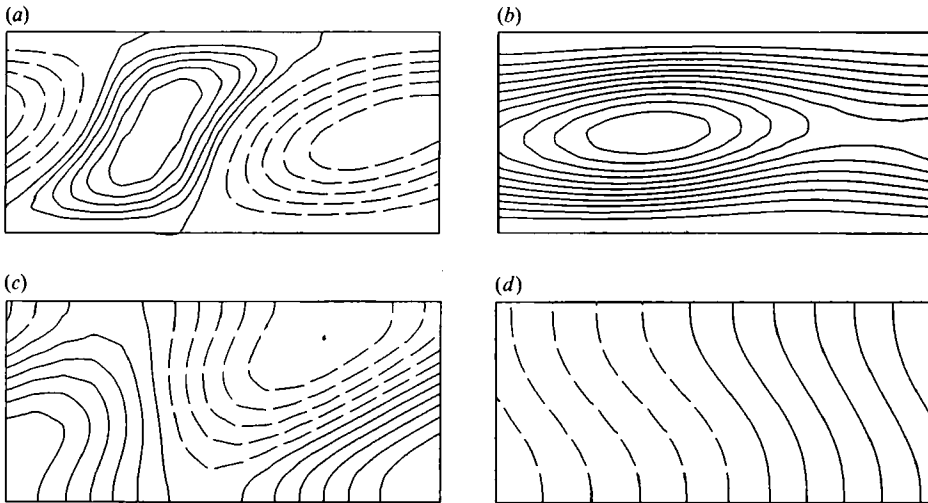
FIGURE 3. Stream functions for (a) secondary flow and (b) total flow, and isotherms for (c) secondary flow and (d) total flow of a moderately supercritical case for $Pr = 0.027$, $\alpha = 2.7$ and $Gr = 11\,700$. The solid lines denote positive values and the dashed lines negative values.

and another that describes the secondary flow. The solution method follows that of Marcus (1984). We have used it previously (Kuo & Korpela 1988; Wang & Korpela 1989; Chait & Korpela 1989) and found it to give excellent accuracy. By forcing the flow to be two-dimensional the appearance of longitudinal rolls is prevented. This way one can study the stability of the equilibrium states even under conditions that might favour the longitudinal rolls. One of these equilibrium states is shown in figure 3 at the condition $Gr = 11\,700$ and the wavenumber $\alpha = 2.7$.

3. Secondary instability

To carry out the analysis of the secondary flow stability, the variables are again split into base flow and secondary flow parts. In addition a small perturbation is added. This split then takes the form

$$u = u_b + u_s + u_p, \quad v = v_s + v_p, \quad w = w_p, \\ P = P_b + P_s + P_p, \quad T = T_b + T_s + T_p, \tag{3.1}$$

where the variables with subscript b satisfy the governing equations for the base flow and the ones with subscript s satisfy those for the secondary flow. At this stage both the base flow and the secondary flow variables are known functions of the coordinates, so their combination can be called a new base state and the linear stability analysis of this new flow can be carried out.

After substituting the variables in (3.1) into (2.1)–(2.3), subtracting the governing equations for the base flow and the secondary flow from them, and neglecting products of disturbance quantities denoted by subscript p in (3.1), the following set of equations is obtained:

$$\partial u_p/\partial x + \partial v_p/\partial y + \partial w_p/\partial z = 0, \tag{3.2}$$

$$\frac{\partial u_p}{\partial t} + Gr v_p \frac{\partial u_b}{\partial y} + Gr\left(u_p\frac{\partial}{\partial x} + v_p\frac{\partial}{\partial y}\right)u_s + Gr\left(u_b\frac{\partial}{\partial x} + u_s\frac{\partial}{\partial x} + v_s\frac{\partial}{\partial y}\right)u_p = -Gr\frac{\partial P_p}{\partial x} + \nabla^2 u_p, \tag{3.3}$$

$$\frac{\partial v_p}{\partial t} + Gr\left(u_p\frac{\partial}{\partial x} + v_p\frac{\partial}{\partial y}\right)v_s + Gr\left(u_b\frac{\partial}{\partial x} + u_s\frac{\partial}{\partial x} + v_s\frac{\partial}{\partial y}\right)v_p = -Gr\frac{\partial P_p}{\partial y} + T_p + \nabla^2 v_p, \tag{3.4}$$

$$\frac{\partial w_p}{\partial t} + Gr\left(u_b\frac{\partial}{\partial x} + u_s\frac{\partial}{\partial x} + v_s\frac{\partial}{\partial y}\right)w_p = -Gr\frac{\partial P_p}{\partial z} + \nabla^2 w_p, \tag{3.5}$$

$$Pr\frac{\partial T_p}{\partial t} + Gr Pr\left(u_p\frac{\partial}{\partial x} + v_p\frac{\partial}{\partial y}\right)T_b + Gr Pr\left(u_p\frac{\partial}{\partial x} + v_p\frac{\partial}{\partial y}\right)T_s \\ + Gr Pr\left(u_b\frac{\partial}{\partial x} + u_s\frac{\partial}{\partial x} + v_s\frac{\partial}{\partial y}\right)T_p = \nabla^2 T_p. \tag{3.6}$$

With insulated top and bottom boundaries, the boundary conditions to be satisfied are

$$u_p = v_p = w_p = \partial T_p/\partial y = 0 \quad \text{at} \quad y = \pm\tfrac{1}{2}, \tag{3.7}$$

with periodicity conditions in the x- and z-directions.

3.1. *Floquet theory*

The coefficients of the unknown functions in (3.2)–(3.6) governing the perturbations depend on the x- and y-coordinates only. Furthermore, some of these coefficients are periodic functions of x. It has been shown by Clever & Busse (1974) and others after them (for a review see Herbert 1988, who also points out the early work by Maseev 1968), that Floquet theory is the proper tool to apply for the analysis of these types of equations. Its application shows that the x-dependence of the perturbation variables can be written as

$$q_p(x, y, z, t) = e^{idx}Q(x, y, z, t), \tag{3.8}$$

where Q is a periodic function of x with the same spatial period as the secondary flow,

and d is a real number called the Floquet exponent. The periodicity of the secondary flow is characterized by the wavenumber α, which dictates the following form for the secondary flow variables:

$$q_s(x, y) = \sum_{m=-M}^{m=M} \bar{Q}_m(y)\, e^{im\alpha x}. \tag{3.9}$$

Since (3.2)–(3.6) are autonomous in z and t the perturbation variables can be written as

$$q_p(x, y, z, t) = \sum_{n=-N}^{n=N} Q_n(y)\, e^{in\alpha x + idx + ibz + \sigma t}. \tag{3.10}$$

In this equation b is the wavenumber characterizing the z-dependence of a three-dimensional flow that may emerge as a result of the secondary transition. The corresponding wavenumber in the primary stability analysis was called β, the different symbols distinguishing whether primary or secondary instabilities are considered. The real part of the complex number σ represents an amplification factor and its imaginary part an oscillation frequency. In the expansions (3.9) and (3.10) the indices m and n should, in principle, vary from minus to plus infinity. In a numerical study the series must be truncated to some suitable low value, which is determined by the requirements of accuracy and the size of the accessible memory in the computer used. The expansions (3.9) and (3.10), when substituted into (3.2)–(3.6) give equations that can be separated, owing to the orthogonality of the Fourier modes, into $2N+1$ coupled equations, one for each of the Fourier modes. This procedure leads to an eigenvalue problem given by the equations

$$i(d + n\alpha)\, U_n + DV_n + ibW_n = 0, \tag{3.11}$$

$$\sigma U_n + Gr[V_n\, Du_b + (U^*\bar{U}_x)_n + (V^*D\bar{U})_n] + Gr[i(d + n\alpha)\, u_b\, U_n + (\bar{U}^*U_x)_n + (\bar{V}^*DU)_n]$$
$$= -iGr(d + n\alpha)\, P_n + [D^2 - (d + n\alpha)^2 - b^2]\, U_n, \tag{3.12}$$

$$\sigma V_n + Gr[(U^*\bar{V}_x)_n + (V^*D\bar{V})_n] + Gr[i(d + n\alpha)\, u_b\, V_n + (\bar{U}^*V_x)_n + (\bar{V}^*DV)_n]$$
$$= -Gr\, DP_n + T_n + [D^2 - (d + n\alpha)^2 - b^2]\, V_n, \tag{3.13}$$

$$\sigma W_n + Gr[i(d + n\alpha)\, u_b\, W_n + (\bar{U}^*W_x)_n + (\bar{V}^*DW)_n] = -ibGr\, P_n + [D^2 - (d + n\alpha)^2 - b^2]\, W_n, \tag{3.14}$$

$$Pr\, \sigma T_n + Gr\, Pr[(U_n) + V_n\, DT_b] + Gr\, Pr[(U^*\bar{T}_x)_n + (V^*D\bar{T})_n]$$
$$+ Gr\, Pr[i(d + n\alpha)\, u_b\, T_n + (\bar{U}^*T_x)_n + (\bar{V}^*DT)_n] = [D^2 - (d + n\alpha)^2 - b^2]\, T_n, \tag{3.15}$$

where D denotes d/dy and an asterisk relates to one of the convolution products

$$\left.\begin{array}{c} (\bar{Q}^*Q)_n = \sum_{\substack{p+q=n \\ |p| \leqslant M, |q| \leqslant N}} \bar{Q}_p Q_q, \qquad (\bar{Q}_x^*Q)_n = \sum_{\substack{p+q=n \\ |p| \leqslant M, |q| \leqslant N}} ip\,\alpha\bar{Q}_p Q_q, \\[2mm] (\bar{Q}^*Q_x)_n = \sum_{\substack{p+q=n \\ |p| \leqslant M, |q| \leqslant N}} i(d + q\alpha)\, \bar{Q}_p Q_q. \end{array}\right\} \tag{3.16}$$

The resolution of the y-dependence of the perturbation variables is still needed. This is done by a K-term expansion in Chebyshev polynomials. As a result a $5K(2N+1)$ matrix equation is obtained, the factor 5 arising from the complete system consisting of continuity, three components of momentum, and the energy equations.

3.2. *Symmetry considerations*

From (2.1) and (2.2) a symmetry of the base flow can be established by a coordinate transformation as

$$u_{\rm b}(y) = -u_{\rm b}(-y), \quad T_{\rm b}(x,y) = -T_{\rm b}(-x,-y). \qquad (3.17)$$

Similarly, the equations governing the secondary flow have solutions that obey the following centro-symmetry properties:

$$\left. \begin{aligned} u_{\rm s}(x,y) &= -u_{\rm s}(-x,-y), \quad v_{\rm s}(x,y) = -v_{\rm s}(-x,-y), \\ T_{\rm s}(x,y) &= -T_{\rm s}(-x,-y), \quad P_{\rm s}(x,y) = P_{\rm s}(-x,-y). \end{aligned} \right\} \qquad (3.18)$$

Since the secondary flow is periodic in x, the periodic structure was shifted in such a way that the stagnation point at the centre of a cell coincides with the origin of the coordinates.

The governing equations of the secondary stability, defined by (3.2)–(3.6) are also seen to have certain symmetries. These are given by

$$\left. \begin{aligned} u_{\rm p}(x,y,z) &= -u_{\rm p}(-x,-y,z), \quad v_{\rm p}(x,y,z) = -v_{\rm p}(-x,-y,z), \\ w_{\rm p}(x,y,z) &= w_{\rm p}(-x,-y,z), \\ P_{\rm p}(x,y,z) &= P_{\rm p}(-x,-y,z), \quad T_{\rm p}(x,y,z) = -T_{\rm p}(-x,-y,z), \end{aligned} \right\} \qquad (3.19)$$

and

$$\left. \begin{aligned} u_{\rm p}(x,y,z) &= u_{\rm p}(x,y,-z), \quad v_{\rm p}(x,y,z) = v_{\rm p}(x,y,-z), \\ w_{\rm p}(x,y,z) &= -w_{\rm p}(x,y,-z), \\ P_{\rm p}(x,y,z) &= P_{\rm p}(x,y,-z), \quad T_{\rm p}(x,y,z) = T_{\rm p}(x,y,-z). \end{aligned} \right\} \qquad (3.20)$$

Following Klaassen & Peltier (1989) the following results can be derived as a result of these symmetries.

(i) If the eigenvalue σ and a corresponding eigenfunction $[U_n(y), V_n(y), W_n(y), P_n(y), T_n(y)]$ are associated with the set of parameters (α, d, b), then σ^* and its associated eigenfunction $[U_n^*(-y), V_n^*(-y), W_n^*(-y), -P_n^*(-y), T_n^*(-y)]$ correspond to the same set of parameters. This means that in the original spectrum the eigenvalues are either real or they appear as complex-conjugate pairs.

(ii) If σ is an eigenvalue corresponding to (α, d, b) and the eigenfunction $[U_n(y), V_n(y), W_n(y), P_n(y), T_n(y)]$ corresponds to it, then σ is also an eigenvalue for $(\alpha, d, -b)$ with an eigenfunction $[U_n(y), V_n(y), -W_n(y), P_n(y), T_n(y)]$. This means that corresponding to an oblique wave with a wavevector inclined to the left of the x-axis there is a similar oblique wave with a wavevector inclined to the right by an equal amount.

(iii) If σ is an eigenvalue corresponding to (α, d, b) and the eigenfunction $[U_n(y), V_n(y), W_n(y), P_n(y), T_n(y)]$ corresponds to it, then σ is also an eigenvalue for $(-\alpha, d, b)$ with an eigenfunction $[U_{-n}(y), V_{-n}(y), W_{-n}(y), P_{-n}(y), T_{-n}(y)]$.

(iv) If σ is an eigenvalue corresponding to (α, d, b) and the eigenfunction $[U_n(y), V_n(y), W_n(y), P_n(y), T_n(y)]$ corresponds to it, then σ is also an eigenvalue for $(\alpha, -d, b)$ with an eigenfunction $[-U_{-n}(-y), -V_{-n}(-y), W_{-n}(-y), P_{-n}(-y), -T_{-n}(-y)]$. Properties (iii)–(iv) show that waves can appear in the flow that travel in oblique directions in such a way that they can be identified as right- or left-travelling

waves with respect to the x-direction. For stationary solutions these properties allow the interpretation of negative wavenumbers as being associated with waves that are shifted in phase 180° from the corresponding positive ones.

(v) The Floquet expansion (3.10) is invariant under the transformation from (α, d, b) to $(\alpha, d + k\alpha, b)$, where k is an integer. This is a consequence of the sums extending to infinity, which allows a renumbering of the indices without affecting the form of the expansion. This means that oblique waves exist in the flow, not singly, but as an infinite set. When d is an integral fraction of α, the sum of such partial waves forms a periodic wave with a wavelength equal to $2\pi/d$.

(vi) Properties (iv) and (v) show that $\sigma(\alpha - d, b) = \sigma(d, b)$, from which it follows that only the range $0 \leqslant d \leqslant \frac{1}{2}\alpha$ need be considered.

As emphasized by Klaasen & Peltier (1989) the parameter b specifies the periodicity of the perturbation in the spanwise direction, but a similar interpretation is not possible for the parameter d. For each value of d in the range $-\frac{1}{2}\alpha < d \leqslant \frac{1}{2}\alpha$ there exists a discrete spectrum of wavevectors and the wavenumber of the partial wave associated with the index n in this spectrum is given by $d + n\alpha$. In such a wave system the relative amplitudes of the partial waves have fixed relations that can be determined from the components of the eigenfunctions.

3.3. *Tests of numerical resolution*

To carry out the secondary stability analysis the secondary flow was first determined by expanding the variables in the y-direction in a Chebyshev series with either 17 or 33 collocation points. In the x-direction the number of Fourier collocations used was either 16 or 32. This corresponds to $M = 8$ or 16 in (3.9). Most of the computations of the secondary flow were carried out at the lower resolution. This was sufficient for an accurate determination of secondary stability characteristics. More notable differences were observed if a secondary flow that had not yet quite reached a steady state was used in the secondary stability calculation.

With an adequately resolved steady secondary flow established the equations (3.11)–(3.15) were solved by a collocation method again using Chebyshev polynomials as expansion functions in y. This gives a $5K(2N+1)$ matrix governing the secondary stability of the flow. The eigenvalues of this matrix were determined by the complex QR-algorithm. The largest value used for N was 2, corresponding to five Fourier modes. Some of the elements of the matrix arise from the convolution sums. For these sums the number of Fourier modes needed from the secondary flow calculation is $4N+1$. Thus at least nine Fourier modes ought to be used to resolve the secondary flow to get this resolution for the secondary stability calculation. As stated, 16 or 32 Fourier modes were used to calculate the secondary flow. Of these 9 were kept for determining the secondary stability.

Actually, it is possible to use fewer terms and still get the qualitative behaviour right. To test this, Chait & Korpela (1989) determined the growth rates by first resolving the secondary flow with 16 Fourier modes and using either one, three, or five of these to represent the secondary flow in the stability calculation. Only the inclusion of five modes gives a consistent representation between the number of Fourier modes used from the secondary flow calculation and the three modes they considered for the perturbations. They also tested how the number of Chebyshev modes in the secondary flow calculation influences the results by varying K from 7 to 17, while keeping five Fourier modes. Whenever K was greater than 13, they saw little reason to increase it more.

Further convergence tests were conducted. Using 17 Chebyshev and 5 or 9 Fourier

α	Gr	d	b	Lower resolution		Higher resolution		Nagata & Busse	
				σ_r	σ_i	σ_r	σ_i	σ_r	α_i
2.6	8000	0	2.0	-8.081	10.44	-8.148	10.47	-9.17	8.3
2.6	8000	1.3	2.0	-6.913	0	-7.086	0	—	—
2.6	8250	—	—	—	—	—	—	LBS	
2.6	8300	1.3	1.5	0.9183	0	0.2079	0	—	
2.6	8500	0	1.6	-0.1246	14.57	-0.5411	15.05	—	
2.6	8580	—	—	—	—	—	—	LBO	
2.6	10000	0	2.0	8.173	23.00	7.132	25.44	7.5	26.25
2.6	10000	1.3	2.0	9.050	0	5.247	0	5^+	0

TABLE 1. Comparison of the growth rate and oscillation frequency calculated with two resolutions and the calculation by Nagata & Busse (1983) for a vanishing Prandtl number. The lower resolution includes three Fourier modes in the x-direction and 17 Chebyshev modes in the y-direction. The higher resolution includes five Fourier modes and 17 Chebyshev modes. The Prandtl number used in our calculation is 10^{-5}. The lower bound for the Grashof number of the subharmonic resonance is denoted by LBS, and LBO, denotes the lower bound for the Grashof number of the oscillatory instability.

modes to represent the secondary flow in a secondary stability calculation, comprising either three or five Fourier modes for the perturbations, the growth rates for $Pr = 10^{-5}$ were calculated in order to compare the results with those obtained by Nagata & Busse (1983) for a vanishing Prandtl number. The results are shown in table 1. They show that significant differences still exist between the results with five Fourier modes for the perturbation variables and those when three Fourier modes are used. It was the result of this test that led us to decide that the higher resolution was needed for the subsequent calculations. This gives a 425×425 matrix eigenvalue problem. To solve it takes 9.6 s on Cray XMP-28. This can be reduced by 30% if the continuity equation is used to eliminate the z-component of velocity and the eigenvalues of the resulting 340×340 matrix are then found.

The property (vi) introduced in the last section was neither exploited in the calculations of Chait & Korpela (1989), nor apparently in those of Nagata & Busse (1983). If it had been used, the figures for the growth rates in those studies would show the proper symmetries. The asymmetry was caused by using the range $0 < d < \alpha$ as the fundamental interval, rather than $-\frac{1}{2}\alpha < d < \frac{1}{2}\alpha$ for determining the growth rates. In the latter case the modes retained, when N is fixed, represent the $2N+1$ lowest ones. If the value of d is varied in the range $0 < d < \alpha$, then whenever $d > \frac{1}{2}\alpha$ one higher-order mode is included in the truncated expansion at the expense of a lower-order one. This leads to inaccuracies, particularly because the series used are truncated at quite low order. After completion of few tests of this kind, the growth rates were calculated only for the interval $0 < d < \frac{1}{2}\alpha$.

4. Results

The aim of this work was to determine the stability characteristics of the secondary flow. Since the secondary flow is two-dimensional and it was calculated as an initial value problem, disturbances that arise as a result of machine roundoff can serve as a source of instability. A stable calculation of the secondary flow thus indicates that the flow with the given wavelength of the secondary flow is stable to a class of two-dimensional disturbances with a wavelength that is an integral fraction
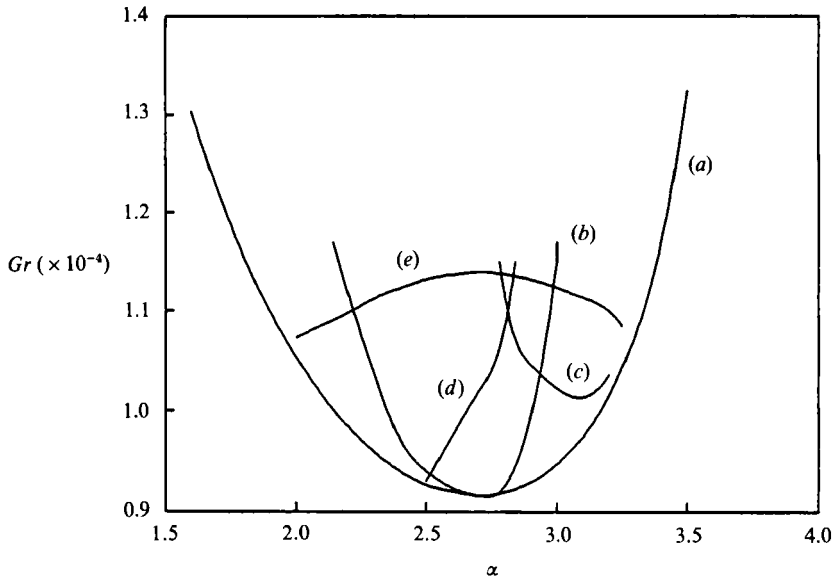
FIGURE 4. Stability regime of the two-dimensional transverse flow for $Pr = 0.027$. The outmost curve (a) indicates the results of a primary stability analysis. The region of stable flow is bounded by: (b) the Eckhaus instability boundary from below, (c) the subharmonic resonance from the right and (d) the combination resonance from left. The boundary of the onset of the oscillatory instability (e) is also shown.

of the fundamental wavelength of the secondary pattern. From this it does not follow, however, that the flow is stable to all two-dimensional disturbances that are smaller than the fundamental, because waves other than those whose wavelengths are an integral fraction of the fundamental wavelength do not fit properly into the fundamental interval. Thus it is possible that the flow could be unstable to classes of disturbances with wavelength smaller than the fundamental one. By considering a larger computational domain into which one can fit more than one period of a wave, one can in principle increase the class of disturbances which can be tested. Doing so one finds, however, that the primary instability mode that favours cells of the critical wavelength causes the flow in a sufficiently long cavity to break up into that cellular structure in which the wavelength is close to the critical one.

It turns out that there are other instability mechanisms at work that limit the range of stable waves more than the mechanism just described. For this reason this kind of instability is not of the greatest concern. In fact, the investigation can be limited to modes that have wavelengths close to the critical. Accordingly, with the critical wavenumber for mercury equal to 2.7, only the range $1.9 < \alpha < 3.2$ was considered and the Grashof number was varied in the range $9157 < Gr < 11700$, the lower end denoting the critical Grashof number of the primary instability. A summary of the investigation is shown in figure 4. It shows five neutral curves. The outermost one is the neutral curve of the primary instability, one shows the *Eckhaus* instability boundary, one the *subharmonic* resonance, and another is associated with *combination resonance*. The last curve, showing the onset of *oscillatory* instability, is above the others and does not directly come into a discussion of the range in which stable transverse cells can exist.
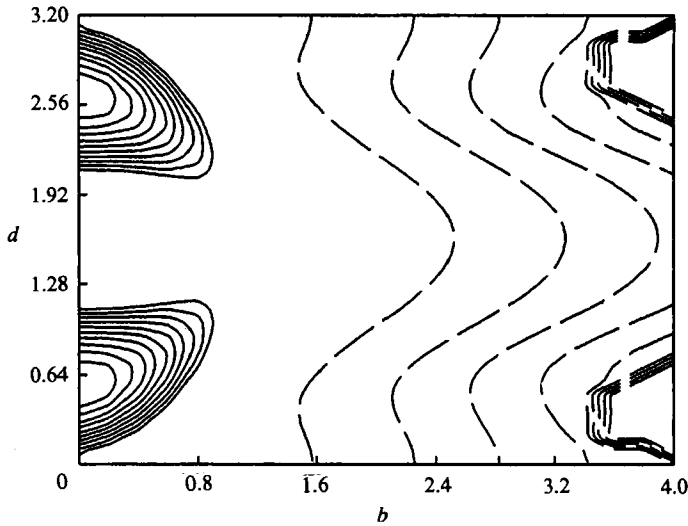
FIGURE 5. The growth rate for the Eckhaus instability as a function of b and d for $Gr = 10\,200$ and $\alpha = 3.2$. The maximum growth rate is 2.847.

4.1. *Eckhaus instability*

It was shown by Eckhaus (1965) that a secondary flow can lose its stability by a three-wave interaction mechanism. Of the many possible wave interactions, the important one, which his theory addresses, is between the first harmonic of the fundamental and two so-called sideband waves, with wavelengths such that one is larger and the other smaller than the fundamental and with an average wavelength equal to the wavelength of the fundamental. A similar mechanism has been shown by Benjamin & Feir (1967) to be at work in water waves and in that context the instability goes by the name of the discoverers. It was Stuart & DiPrima (1978) who showed the connection between the Eckhaus and the Benjamin–Feir resonance mechanisms. These studies rely on perturbation methods which allow an amplitude equation to be derived. It shows how the low-order harmonics of the spatially periodic base flow interact with the sideband waves, and allows evolution of the sideband waves to be followed.

The Eckhaus instability is a two-dimensional one and thus corresponds to disturbances with $b = 0$. In figure 5 the growth rate of the least stable mode at $\alpha = 3.2$ and $Gr = 10\,200$ is shown as a function of b and d. This state is close to the right branch of the primary stability curve. From figure 5 it is seen that strongest decay is at $d = \frac{1}{2}\alpha$, the regions of positive growth are located symmetrically about $d = \frac{1}{2}\alpha$, and that the two maxima are along $b = 0$. If on the interval $\frac{1}{2}\alpha < d < \alpha$ the location of the maximum is called d_0, the other maximum is then located at $d = \alpha - d_0$. The plot can be extended periodically to larger and smaller values of d and by reflection to negative values of b.

The results indicate that in a flow subjected to two-dimensional disturbances a countably infinite set of partial waves can grow. The growth, according to Eckhaus, is a result of a three-wave interaction and the principal interaction is among the first harmonic of the fundamental with the wavenumber 2α, the upper sideband wave with the wavenumber $2\alpha - d_0$, and the lower sideband wave with a wavenumber d_0. This interaction leads to the loss of stability of the fundamental and the growth of the sideband waves. Eckhaus theory shows that of the two waves in the amplified
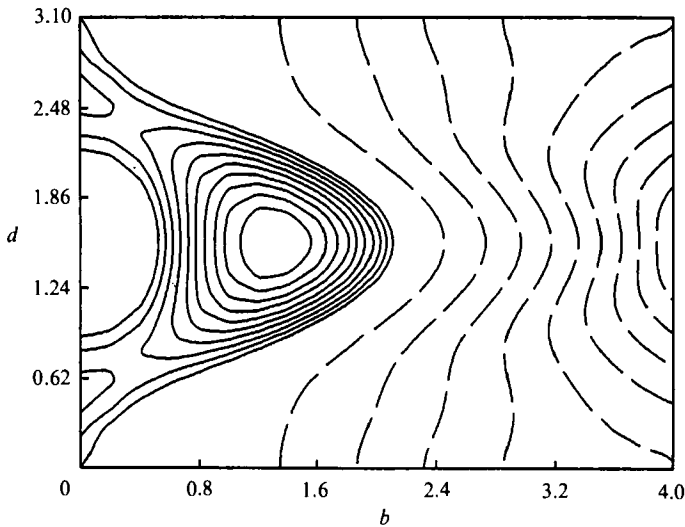
FIGURE 6. The growth rate for the Eckhaus instability and the subharmonic resonance as a function of b and d for $Gr = 11200$ and $\alpha = 3.1$. The maximum growth rate is 6.131.

sidebands the wave in the lower sideband dominates. The wave with the maximum growth rate in the lower sideband has a wavenumber close to that of the critical wavenumber of the primary instability. This is true only for states that are not too close to the boundary of the Eckhaus curve, for exactly at the boundary the wavenumber of the sideband waves approaches that of the state tested for instability. Thus in general the flow tends to return to what could be called its 'natural state', characterized by the wavenumber d_0, which is close to the critical wavenumber of the primary instability.

Reducing the wavenumber to 3.1 and increasing the Grashof number to 11200 yields the amplification plot shown in figure 6. In comparing this to figure 4 it can be seen that both the Eckhaus and the subharmonic mechanisms (discussed in the next section) manifest themselves at this state, the Eckhaus mechanism being the weaker of the two.

The size and shape of the partial waves are shown in figure 7. In that figure the normalized eigenfunctions for different Fourier modes at $Gr = 10200$, $\alpha = 3.2$, $d = 0.6$ and $b = 0$ are plotted. The lower sideband wave has an amplitude one order larger than the upper sideband wave, which matches the analysis by Eckhaus. The amplitude of the longest wave with a wavenumber equal to $\alpha - d_0$ is second largest, followed first by the upper sideband wave and then by the other shorter waves.

The behaviour of the flow near the left branch of the Eckhaus curve is more complicated. There the maximum amplification rate of the growing waves does not occur at $b = 0$. The unstable waves are detuned modes in the sense that the wavenumbers at which the maximum growth takes place correspond neither to $d = 0$ nor to $d = \frac{1}{2}\alpha$, the two values that are singled out for favoured status owing to their common appearance in instability mechanisms. They are discussed further below. The Eckhaus curve drawn is for the onset of instability of waves with $b = 0$ and thus it corresponds to a strictly two-dimensional mechanism.

The Eckhaus instability, in the end, does not have an important function for predicting the behaviour of an actual flow in a laboratory, for whereas in our theoretical study the wavelength could be chosen at will and we could this way carry
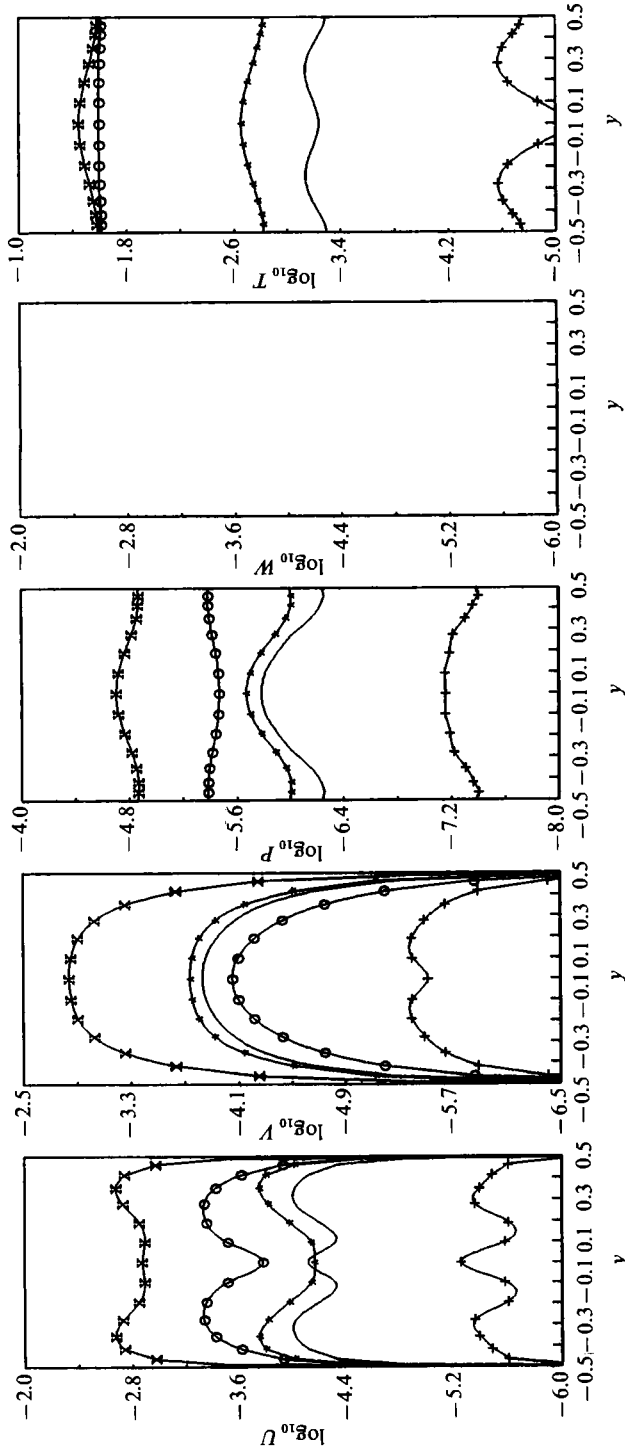
FIGURE 7. The amplitudes of the eigenfunctions for $Gr = 10200$, $\alpha = 3.2$, $d = 0.6$ and $b = 0$: $+$, $n = 2$; $*$, $n = 1$; $\bigcirc$, $n = 0$; $\times$, $n = -1$; and ———, $n = -2$. The n identify the partial waves in equation (3.10), with wavenumbers in the x-direction equal to $n\alpha + d$.
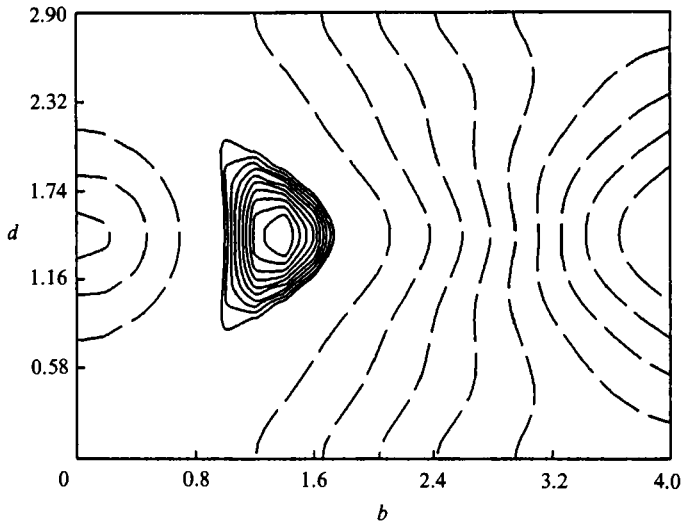
FIGURE 8. The growth rate for the subharmonic resonance as a function of b and d for $Gr = 11\,700$ and $\alpha = 3.0$. The maximum growth rate is 5.401.

out a parametric study of waves of various wavelengths, in a laboratory this is not so readily accomplished. In fact, the naturally growing wave has a wavelength near the middle of the region of stable waves and by increasing the Grashof number the important secondary instability mechanism is the one that limits the transverse cells from above in figure 4. There are three curves that do this and it is to them that we now turn our attention.

4.2. Subharmonic resonance

Kelly (1967) was the first to note that an instability via subharmonic resonance is possible. He studied the stability of a shear layer in which this mechanism is a two-dimensional one. A three-dimensional subharmonic mechanism was discovered by Herbert (1983) for boundary-layer flows and, according to his theory, is responsible for the staggered pattern of lambda-vortices that have been identified in these flows. The same mechanism was identified by Nagata & Busse (1983) to be at work in natural convection in a vertical slot.

The distinguishing feature of the subharmonic resonance is that a wave with a wavenumber equal to $\frac{1}{2}\alpha$ is amplified the most. The amplification rates in figure 8 show this. The maximum amplification rate corresponds to $b = 1.35$ and this value depends strongly on neither α nor Gr. That the solution with a Floquet exponent equal to $\frac{1}{2}\alpha$ corresponds to a periodic solution with this wavenumber can be easily seen by substituting this value of d into (3.10) and combining terms. Doing so allows this equation to be put into a form in which d is absent, α is replaced by $\frac{1}{2}\alpha$, and the index n by $2n + 1$. The periodic extension of the amplitude plot in figure 8 now shows that the subharmonic and its odd harmonics are amplified. These constitute one three-dimensional periodic wave that is stationary since the imaginary part of the growth rate is zero.

We have plotted in figure 9 the eigenfunctions for $Pr = 0.027$, $Gr = 11\,700$, $d = \frac{1}{2}\alpha = 1.5$, and $b = 1.35$. The dominance of the subharmonic is clear from this figure. In figure 10 the velocity vectors in the (x, y)-plane at different z-locations, obtained from set of eigenfunctions, show the form of the flow arising from subharmonic resonance. The structure of this flow can most simply be visualized by
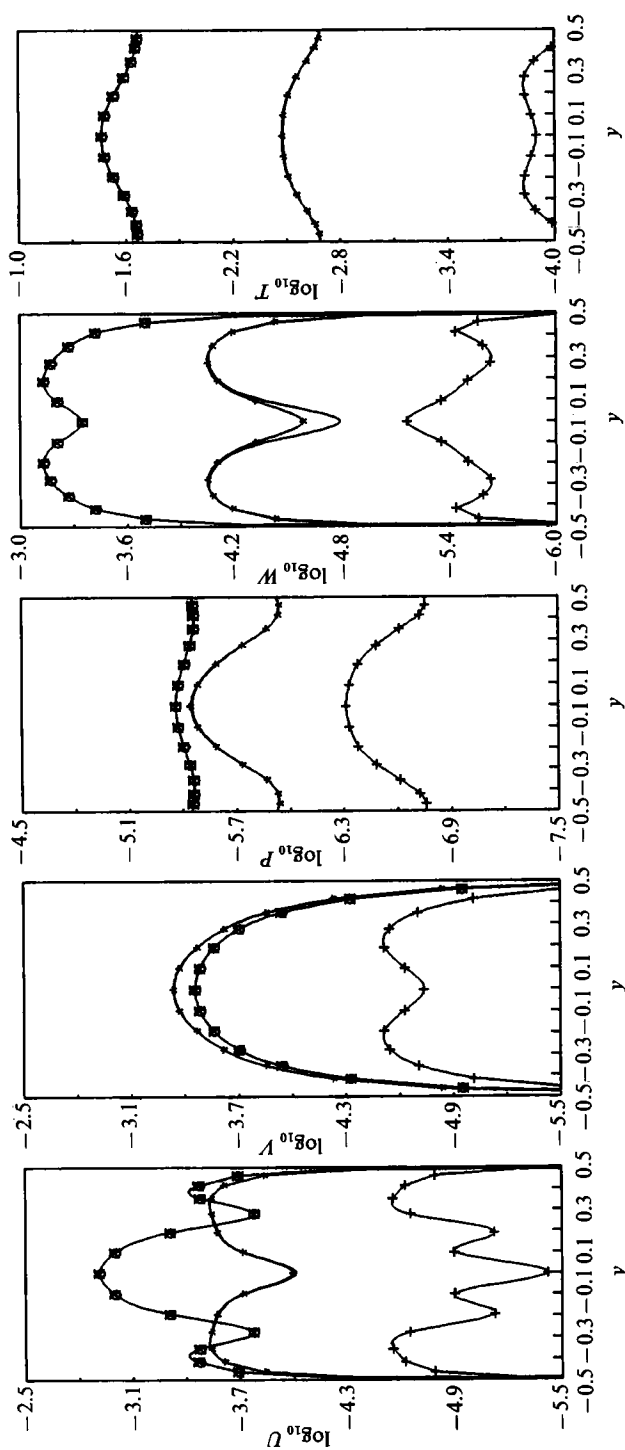
FIGURE 9. The amplitudes of the eigenfunctions for $Gr = 11\,700$, $\alpha = 3.0$, $d = 1.5$ and $b = 1.35$: $+$, $n = 2$; $*$, $n = 1$; $\bigcirc$, $n = 0$; $\times$, $n = -1$, and $\underline{\quad\quad}$, $n = -2$. The n identify the partial waves in equation (3.10), with wavenumbers in the x-direction equal to $n\alpha + d$. The modes $n = 0$ and $n = -1$ coincide, as do the modes with $n = 1$ and $n = -2$.
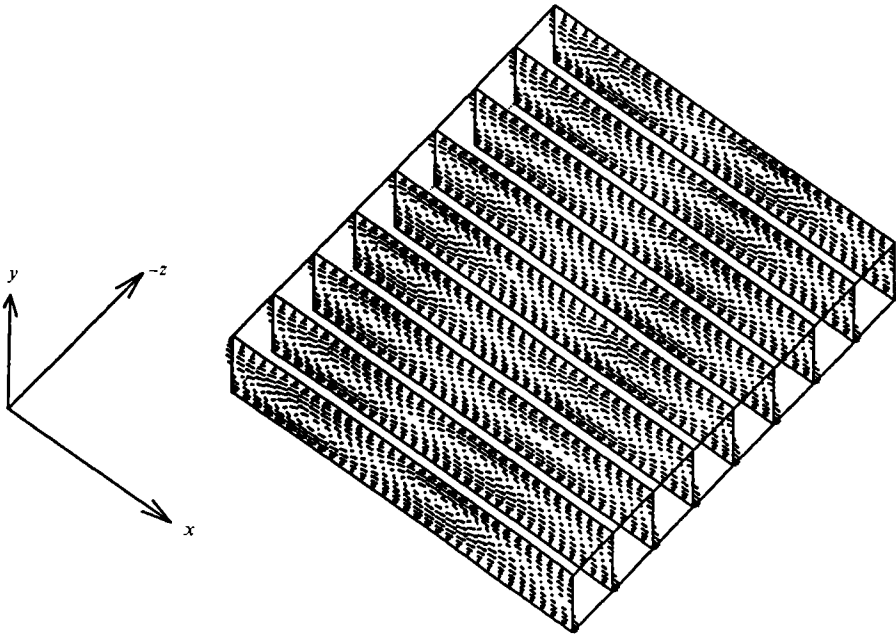
FIGURE 10. Velocity vectors of the total flow on the (x, y)-plane for $Gr = 11\,700$, $d = \frac{1}{2}\alpha = 1.5$ and $b = 1.35$. The distance between consecutive planes is uniform and equal to $\frac{1}{8}\lambda_z$.

considering what the cell axes do in a plan view, i.e. on an (x, z)-plane. If one lets the cell axes be described by a sine wave, assumes that all the axes lie on the midplane between the plates, and draws one of them on this midplane, then the next cell axis, located downstream by a distance π/α, is in the spanwise direction 180° out of phase with the former and its peaks are aligned with the valleys of the first one. Continuing this process by drawing the next one, similarly out of phase with the second one, gives a qualitative picture of the relative position of the cell axes. Although this simplified picture does not tell us how the cell axes migrate with regard to the y-position, it is in accordance with the observation of Herbert (1983) that in a boundary layer the staggered pattern of lambda-vortices fits the theory of subharmonic resonance. In a confined flow as considered here this structure forms also as a result of the flow field being such that the variation of the variables in the z-direction is sinusoidal. Thus the cell axes have a tendency to be drawn together on one z-plane and pushed apart one half of a wavelength later. This undulation produces a staggered pattern in a plan view.

From figure 4 one sees that the subharmonic mechanism is important only on roughly the right half of the unstable states as defined by the neutral curve of the primary instability. On the left-hand side the curve identifying an instability arising from combination resonance limits the domain of stable transverse cells from above. Because we do not know how the wavelength of the transverse cells actually varies with the amplitude of convection, we cannot *a priori* determine the locus of states through which the system passes as the Grashof number is increased. This locus may cross the subharmonic branch, but it may equally well cross the curve marking the detuned modes that give rise to combination resonance. In the next section we discuss the characteristics of these modes.
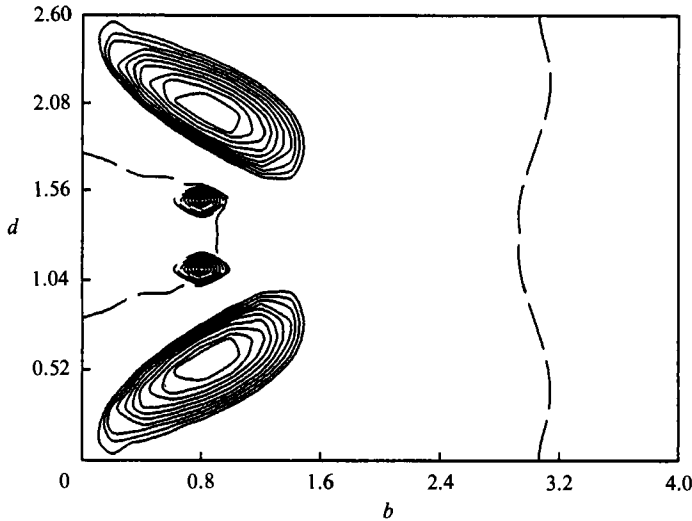
FIGURE 11. The growth rate for the modes arising from combination resonance as a function of b and d for $Gr = 11\,500$ and $\alpha = 2.6$. The maximum growth rate is 2.002.

4.3. *Combination resonance*

On the left side in figure 4 the stable transverse cells lose their stability as the Grashof number is increased, with the instability setting in as a system of oblique waves. Regarding terminology, the fact that both d and b differ from zero suggests the name oblique modes. The symmetries in the base flow and the transverse cells lead to the occurrence of paired modes that are detuned by an equal amount, but in the opposite sense. These combined paired modes resonate with the harmonics of the secondary flow to bring about an instability (Herbert 1988). A sample plot of the amplification rates of these detuned modes is given in figure 11, for $\alpha = 2.6$ and $Gr = 11\,500$. The maximum growth takes place near $d = 0.59$ and $b = 0.88$, and in symmetrical location about the $d = \frac{1}{2}\alpha$ line. Again because of the periodic extension of this plot for both positive and negative values of d and the extension of the figure by reflection to negative values of b, an infinite number of wave interactions can be identified. Of these the principle ones, in analogy with the Eckhaus mechanism, involve the waves with wavenumbers $(2\alpha-d_0, -b)$, (d_0, b), and the first harmonic with wavenumbers $(2\alpha, 0)$. The other similar set with the sign of b changed differs from this only by having the wavevectors of the corresponding waves inclined in the opposite direction of the x-axis than in the first set. Since the value of d_0 is not necessarily equal to α/n for some n, these waves do not in general form a periodic pattern.

The normalized amplitudes of a set of eigenfunctions for different Fourier modes at $\alpha = 2.6$, $Gr = 11\,500$, $d = 0.52$ and $b = 0.8$ are shown in figure 12. These are characterized by the disappearance of the dominance of a single mode. This is an interesting result, because it brings out the possibility that some other triad interaction may be as important as the one involving the upper and lower sideband waves. One such set consists of waves having wavenumbers $(\alpha - d_0, b_0)$ and $(d_0, -b_0)$ interacting with the fundamental with $(\alpha, 0)$. The reason for choosing this triad as possibly being important is that it involves waves longer than the fundamental and for that reason it should draw energy better from the mean flow than the very short waves which are generally fed from immediately larger modes.

Close to the left branch of the Eckhaus boundary a different kind of combination
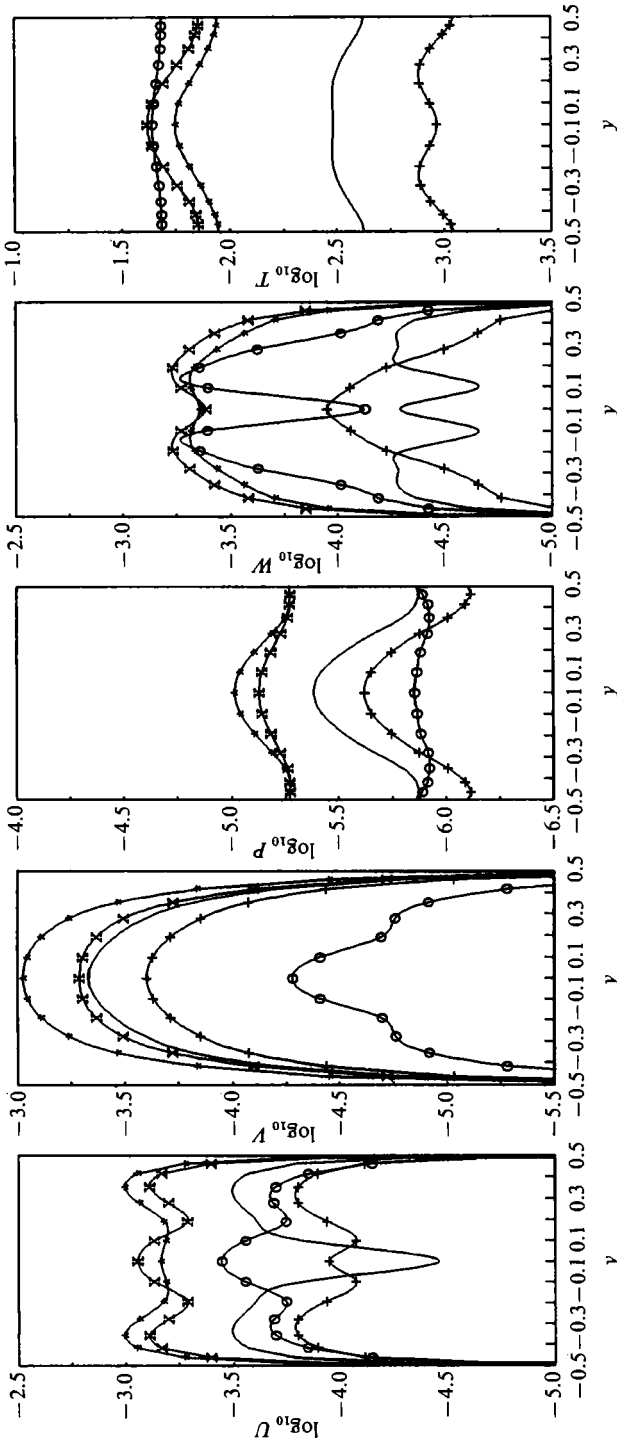
FIGURE 12. The amplitudes of the eigenfunctions for $Gr = 11\,500$, $\alpha = 2.6$, $d = 0.52$ and $b = 0.8$: $+$, $n = 2$; $*$, $n = 1$; $\bigcirc$, $n = 0$; $\times$, $n = -1$; and ———, $n = -2$. The wavenumber in the x-direction is $n\alpha + d$.
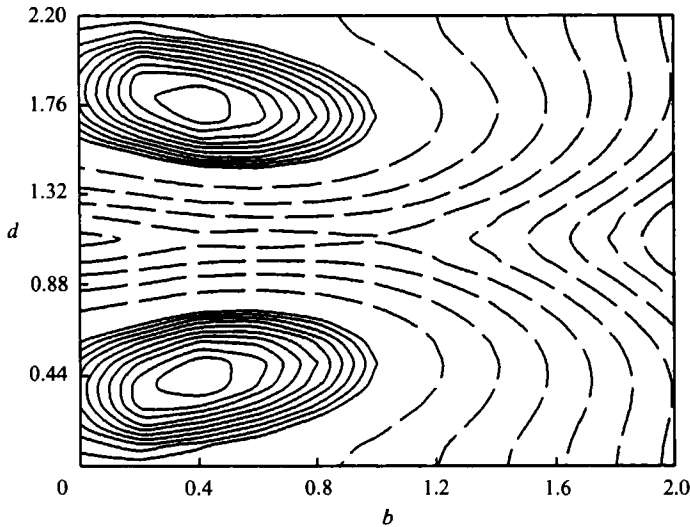
FIGURE 13. The growth rate for the modes arising from combination resonance as a function of b and d for $Gr = 10400$ and $\alpha = 2.2$. The maximum growth rate is 2.166.

resonance dominates. The amplification plot for it is shown in figure 13 at the state $Gr = 10400$ and $\alpha = 2.2$. At this state the region of positive growth includes the $b = 0$ axis. The neutral states for this kind of instability were not traced out, since they are to the left of the curve of the more clearly defined combination resonance.

Should the transverse cells lose their stability by a mechanism involving the combination resonance, the question of how these waves manifest themselves in an experiment is an important one. The theory indicates that the waves should again be stationary, for the most dangerous eigenvalues are purely real. Nevertheless, since the waves are oblique, in an experimental cavity of finite size the interaction of the boundaries may bring in completely new effects. Should the boundary interaction manifest itself as a loss of steadiness of the wave pattern, then this may be an explanation for the appearance of a low-frequency oscillation observed in the experiments of Hung & Andereck (1988). The fluid in the experiment may be trying to adjust itself into a pattern that fits the oblique waves into the cavity, but it cannot find the right form owing to the influence of the boundaries. The only evidence for this view at present is that, according to Hung & Andereck (1988), the power spectrum of the signal for the low-frequency oscillations is reminiscent of drifting large-scale structures.

4.4. *Oscillatory states*

In figure 4 a stability boundary above which oscillatory states are possible is also plotted. Even if this curve lies above both the subharmonic curve and the one characterizing the combination resonance, it does not lie far above them. For this reason, and from what the experiments have shown, it must be considered. A sample amplification plot for the oscillatory states is shown in figure 14. Since the maximum amplification rate for these states occurs for $d = 0$ and $d = \alpha$ the oscillatory states are characterized by the wavenumber pair (α, b). For a small amplitude of the transverse cells these modes have the characteristics of the longitudinal rolls that were identified in the linear stability analysis, the properties of which are discussed in Wang & Korpela (1989) and more fully in Wang (1990). The rolls are realigned by the presence of the transverse cells, but this does not influence their size, since the critical
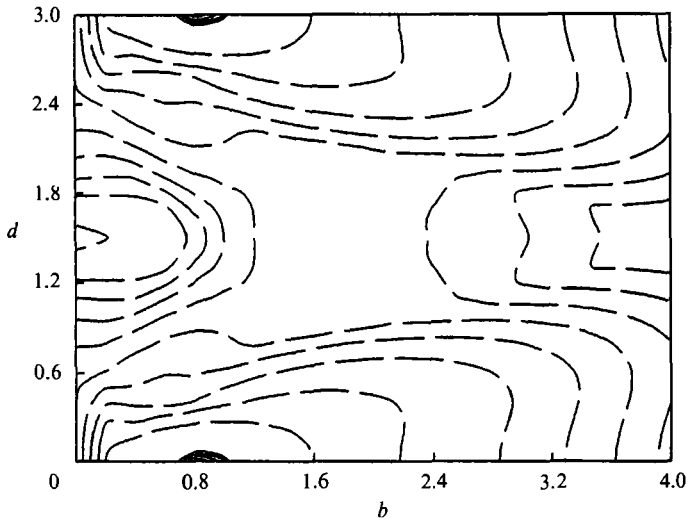
FIGURE 14. The growth rate for the oscillatory instability as a function of b and d for $Gr = 11\,700$ and $\alpha = 3.0$. The maximum growth rate is 0.406 and the oscillation frequency is 40.44.

wavenumber falls into the same range of $0.7 < b < 0.8$ as before. The oscillation frequency is also practically the same as given by the primary stability analysis. Based on the analysis and the experiments of Hung & Andereck (1988) it can be concluded that for the slightly supercritical states that have been investigated neither the presence of transverse cells, nor the staggered cell pattern arising from subharmonic resonance, nor an oblique wave system arising from the combination resonance, distort the base flow sufficiently to suppress this mode of instability.

The influence of the transverse cells is a slight stabilization of the flow. This is evident from the neutral stability curve of the oscillatory modes having being bent upward at the centre. In the absence of transverse cells, these cells are longitudinal, and the primary stability theory requires their neutral states to be independent of α. Thus if the transverse cells were to have no influence on the instability of the oscillatory modes at all, their neutral curve in figure 4 would be a straight horizontal line. Near the neutral curve of the primary stability the onset of the oscillatory rolls matches exactly what the primary stability theory predicts, for the reason that for these states the amplitude of the transverse cells is nil. For supercritical states with a wavelength close to the critical one for transverse cells, the flow is furthest removed from the neutral conditions and thus the amplitude of the secondary cells is largest. It is for these states that the onset of the oscillatory modes has been delayed somewhat.

In figure 15 the amplitudes of a set of eigenfunctions are plotted at the state with $Pr = 0.027$, $Gr = 11\,700$, $\alpha = 3.0$, $d = 0$, and $b = 0.8$. As a result of the symmetry properties the eigenfunctions for positive n are reflections of those for negative n, the eigenfunctions being in general asymmetric. The mean with $n = 0$, however, must be symmetric. By using these eigenfunctions we can construct plots of various quantities associated with the flow. Figure 16 shows the three components of velocity, and the temperature on the planes of symmetry and the cavity midplane. Both the isolines of u-velocity and the temperature show an oblique pattern clearly, consistent with the orientation of the wavevector defined by $(\alpha, b) = (3.0, 0.8)$. Since the flow is time dependent the figures shown are snapshots of the flow which evolves
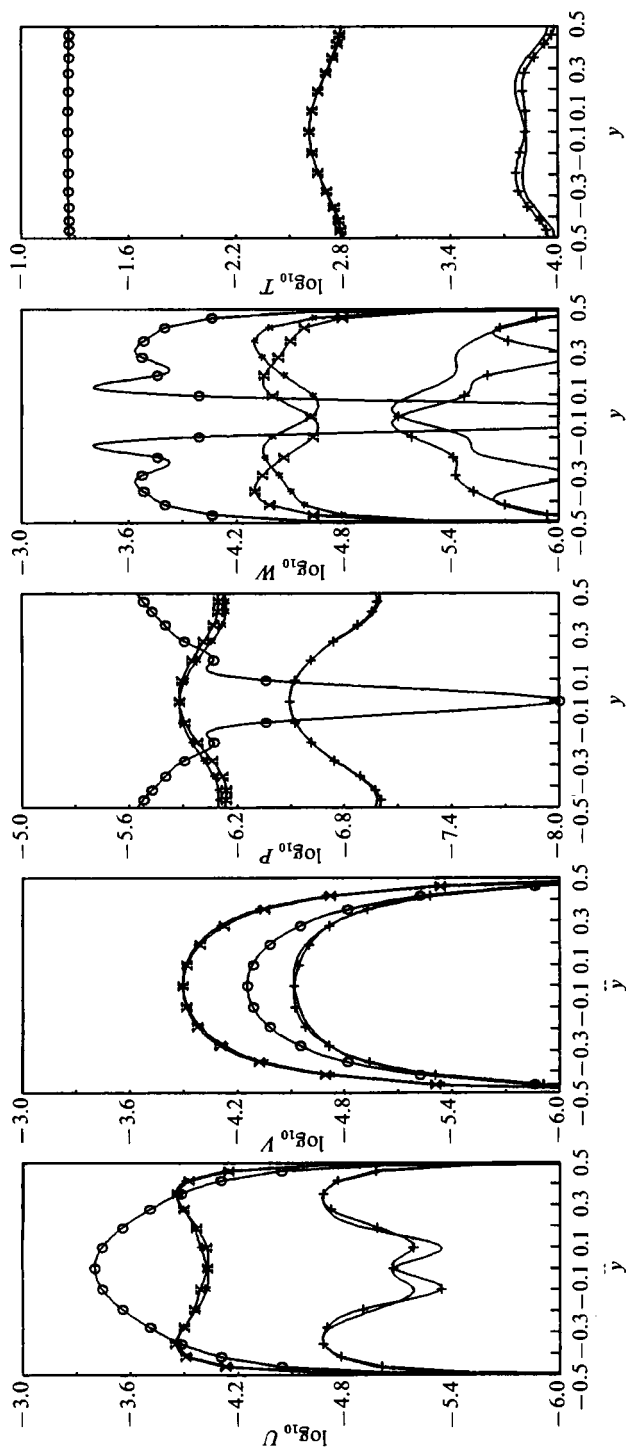
FIGURE 15. The amplitudes of the eigenfunctions for $Gr = 11700$, $\alpha = 3.0$, $d = 0$, and $b = 0.8$: $+$, $n = 2$; $*$, $n = 1$; $\bigcirc$, $n = 0$; $\times$, $n = -1$; and ———, $n = -2$. The wavenumber in the x-direction is $n\alpha + d$.
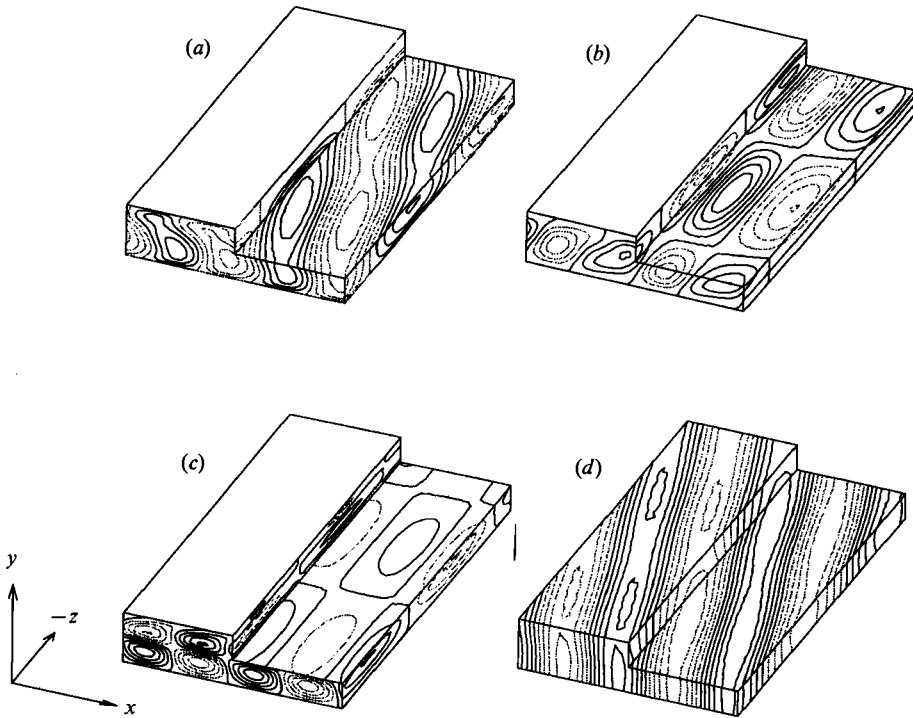
FIGURE 16. Isolines of (a) u-component of velocity, (b) v-component of velocity, (c) w-component of velocity and (d) isotherms for the oscillatory instability for $Gr = 11\,700$, $\alpha = 3.0$, $d = 0$ and $b = 0.8$. Two spatial periods in the x-direction are shown.

periodically in time. With time fixed, however, the z-coordinate can be taken as a time-like variable and these figures are seen to be very similar to those in Wang & Korpela (1989).

5. Conclusions

In this paper we have shown that the transverse cells that develop in a convective flow in shallow cavity as a result of a primary instability become unstable by a secondary instability mechanism involving either a subharmonic resonance or as a combination resonance. At somewhat larger values of the Grashof number an oscillatory instability appears, which is closely related to what the primary stability analysis predicts. In summary, then, if experiments could be carried out for mercury in a cavity that is very large in its horizontal extent, the primary instability would set in as steady transverse cells at $Gr = 9157.6$ and $\alpha = 2.7$. Provided that the wavelength of these cells does not change much with the amplitude of convection a secondary instability would set in as a set of detuned three-dimensional steady modes at about $Gr = 10\,500$. If, however, the wavelength of the transverse cells decreases with amplitude, then the mechanism that brings about the secondary instability would be subharmonic resonance. If either of these instabilities could be suppressed, a longitudinal oscillatory instability would set in at about $Gr = 11\,400$. The experiments of Hung (1989) suggest that such an oscillatory state is in fact reached, but not until $Gr = 18\,490$. We believe that the cause for the delay is the finite horizontal extent of the experimental cavity. That the oscillatory instability is

closely related to the one found from the primary stability analysis follows from the way in which the neutral curve of the oscillatory states approaches the neutral curve obtained from the primary stability analysis. Along the latter curve the amplitude of the transverse cells vanishes and thus the secondary instability analysis must (and it does) give results that are identical to those obtained by analysis of the base state alone. Away from the primary stability curve the secondary instability as oscillatory modes is only slightly delayed, indicating that the transverse cells do not qualitatively change the eigenvalue spectrum obtained from the primary stability analysis and that their quantitative influence on the stability of these modes is small.

Although the experimental support for the existence of oscillatory instabilities is strong, the theory cannot explain the delay in the onset of these modes. Neither does the analysis presented here explain the appearance of low-frequency oscillations seen in the experiments at slightly supercritical Grashof numbers. Whether these are related to the modes that arise by subharmonic or combination resonance that then interact with a cavity of finite aspect ratio remains an open question. We plan to take this up by carrying out fully three-dimensional simulations in a finite cavity in the future.

REFERENCES

BENJAMIN, T. B. & FEIR, J. E. 1967 The disintegration of wave trains on deep water. Part 1. Theory. *J. Fluid Mech.* **27**, 417–430.

CHAIT, A. & KORPELA, S. A. 1989 The secondary flow and its stability for natural convection in a tall vertical enclosure. *J. Fluid Mech.* **200**, 189–216.

CLEVER, R. M. & BUSSE, F. H. 1974 Transition to time-dependent convection. *J. Fluid Mech.* **65**, 625–645.

DRUMMOND, J. E. & KORPELA. S. A. 1987 Multicellular natural convection in a shallow cavity. *J. Fluid Mech.* **148**, 245–266.

ECKHAUS, W. 1965 *Studies in Non-linear Stability Theory*. Springer.

GERSHUNI, G. Z., ZHUKHOVITSKII, E. M. & MYZNIKOV, V. M. 1974 Stability of plane-parallel convective fluid flow in a horizontal layer relative to spatial oscillations. *J. Appl. Mech. Tech. Phys.* **5**, 706–708.

GILL, A. E. 1974 A theory of thermal oscillations in liquid metals. *J. Fluid Mech.* **64**, 577–588.

HART, J. E. 1972 Stability of thin non-rotating Hadley circulations. *J. Atmos. Sci.* **29**, 687–697.

HART, J. E. 1983 A note on the stability of low-Prandtl-number Hadley circulations. *J. Fluid Mech.* **132**, 271–281.

HERBERT, TH. 1983 Secondary instability of plane channel flow to subharmonic three-dimensional disturbances. *Phys. Fluids* **26**, 871–874.

HERBERT, TH. 1988 Secondary instability of boundary layers. *Ann. Rev. Fluid Mech.* **20**, 487–526.

HUNG, M. C. 1989 Transitions in convection of a low Prandtl number fluid Driven by a horizontal temperature gradient. Ph.D. thesis, The Ohio State University.

HUNG, M. C. & ANDERECK, C. D. 1988 Transitions in convection driven by a horizontal temperature gradient. *Phys. Lett.* A **132**, 253–258.

HURLE, D. T. J. 1966 Temperature oscillations in molten metals and their relationship to growth striae in melt-grown crystals. *Phil. Mag.* **13**, 305–310.

HURLE, D. T. J., JAKEMAN, E. & JOHNSON, C. P. 1974 Convective temperature oscillations in molten gallium. *J. Fluid Mech.* **64**, 565–576.

KELLY, R. E. 1967 On the stability of an inviscid shear layer which is periodic in space and time. *J. Fluid Mech.* **27**, 657–689.

KLAASSEN, G. P. & PELTIER, W. R. 1989 The role of transverse secondary instabilities in the evolution of free shear layers. *J. Fluid Mech.* **202**, 367–402.

KUO, H. P. & KORPELA, S. A. 1988 Stability and finite amplitude natural convection in a shallow cavity with insulated top and bottom and heated from a side. *Phys. Fluids* **31**, 33–42.

KUO, H. P., KORPELA, S. A., CHAIT, A. & MARCUS, P. S. 1986 Stability of natural convection in a shallow cavity. In *Eight Intl Heat Transfer Conf. San Francisco*, vol. 4, pp. 1539–1544. Hemisphere.

LAURE, P. 1987 Etude des mouvements de convection dans une cavité rectangulaire soumise à un gradient de température horizontal. *J. Méc. Théor. Appl.* **6**, 351–382.

MARCUS, P. S. 1984 Simulation of Taylor-Couette flow. Part 1. Numerical methods and comparison with experiments. *J. Fluid Mech.* **146**, 45–64.

MASEEV, L. M. 1968 Occurrence of three-dimensional perturbations in a boundary layer. *Fluid Dyn.* **3**, 23–24.

NAGATA, M. & BUSSE, F. H. 1983 Three-dimensional tertiary motions in a plane shear layer. *J. Fluid Mech.* **135**, 1–26.

PIERREHUMBERT, R. T. & WIDNALL, S. E. 1982 Secondary instability of wall bounded shear flows. *J. Fluid Mech.* **114**, 347–385.

ROUX, B., BONTOUX, P. & HENRY, D. 1984 Numerical and theoretical study of different flow regimes occurring in horizontal fluid layers differentially heated. Lecture Notes in Physics, vol. 230, pp. 103–134. Springer.

STUART, J. T. & DIPRIMA, R. C. 1978 The Eckhaus and Benjamin–Feir resonance mechanisms. *Proc. R. Soc. Lond.* A **362**, 27–41.

WANG, T. M. 1990 Secondary stability and three dimensional natural convection in a shallow cavity. Ph.D. thesis, The Ohio State University.

WANG, T. M. & KORPELA, S. A. 1989 Convection rolls in a shallow cavity heated from a side. *Phys. Fluids* A **1**, 947–953.